Citation for published version:
Zhang, Z, Wang, Z & Gursul, I 2020, 'Lift Enhancement of a Stationary Wing in a Wake', *AIAA Journal*, vol. 58, no. 11, pp. 4613-4619. https://doi.org/10.2514/1.J059872

DOI:
10.2514/1.J059872

Publication date:
2020

Document Version
Peer reviewed version

Link to publication

University of Bath

Alternative formats
If you require this document in an alternative format, please contact:
openaccess@bath.ac.uk

General rights
Copyright and moral rights for the publications made accessible in the public portal are retained by the authors and/or other copyright owners and it is a condition of accessing publications that users recognise and abide by the legal requirements associated with these rights.

Take down policy
If you believe that this document breaches copyright please contact us providing details, and we will remove access to the work immediately and investigate your claim.

Download date: 11. May. 2021

Lift Enhancement of a Stationary Wing in a Wake

Z. Zhang[1], Z. Wang[2], and I. Gursul[3]

Department of Mechanical Engineering

University of Bath, Bath, England BA2 7AY, United Kingdom

Abstract

A stationary wing placed in the wake of a bluff body experiences lift enhancement. The quasi-periodic flow in the wake causes excitation of the separated flow in the post-stall conditions. The increase in the time-averaged lift force is associated with the flow separation, leading-edge vortex formation and subsequent reattachment in a process similar to the dynamic stall of oscillating wings. The lift enhancement is maximum for an optimal offset distance from the wake centerline. At the optimal location, potential flow oscillations, rather than the direct impingement of large vortices in the wake, provide the excitation. The smaller amplitude flow oscillations lead to a large separation bubble in the time-averaged sense in the post-stall regime. The delayed flow separation in the wake has a similar mechanism and frequency to those of the active flow control methods for separation. The degree of the lift enhancement is remarkable, given that the wake at a Reynolds number of 50,000 is expected to be highly three-dimensional.

[1] PhD student

[2] Senior Lecturer

[3] Professor, Associate Fellow, AIAA.

Nomenclature

b	span
C_L	mean lift coefficient
c	chord length
f	frequency
K	reduced pitch rate
P	probability
Re	Reynolds number
t	time
U	mean streamwise velocity component
U_∞	freestream velocity
u	instantaneous streamwise velocity component
V	mean cross-stream velocity component
v	instantaneous cross-stream velocity component
x	streamwise distance
y	cross-stream distance
α	angle of attack
ω	spanwise vorticity
rms	root-mean-square
LE	leading-edge

I. Introduction

Aerodynamic surfaces operating in wakes are commonly encountered in various engineering applications and biological flows. Canard-wing configurations in fixed-wing aircraft [1], flight refuelling, aircraft wings in ship airwakes, formation flight [2], oscillating tandem-wing configurations in nature [3] and biomimetic propulsion [4], energy harvesting in bluff body wakes [5], and rotor blades passing through the wakes of stator blades in turbomachinery [6] are some examples. The majority of these cases is governed by the interaction of the unsteady wakes shed from upstream bodies/wings with downstream wings. Even if the wake is turbulent at higher Reynolds numbers, the interaction of highly coherent vortices with the wing determines the mean lift and drag as well as the fluctuating loads. Flow physics of various types of vortex–body interactions, including the case of a Karman vortex street interacting with a downstream surface, have been reviewed by Rockwell [7].

Interaction of a fully developed Karman vortex street with a two-dimensional body at zero angle of attack was investigated at a low Reynolds number range [8]. It was shown that the wavelength λ_∞ in the undisturbed vortex street and the offset distance between the wake centreline and the leading-edge of the body are the two important length scales that have major influence on the details of the interaction, distortion of the vortical structures near the leading-edge as well as unsteady pressure field on the surface of the body. Durgesh et al. [9] reported lift and drag measurements of an airfoil in the near-wake of a bluff body (0.5 to 1.0 chord lengths downstream) at zero offset distance. There was a decrease in the slope of the curve of the time-averaged lift coefficient versus angle of attack. The decrease in the lift slope, which could be significant, was attributed to the smaller dynamic pressure due to the velocity defect in the wake. Similar decrease in the time-averaged lift slope was noted in other experiments in the near-wake and at zero offset distance [10]. There was also a delay of the stall, however the maximum lift coefficient remained nearly the same. In these studies, the Reynolds number of the wake based on the width of the bluff body were on the order of 10^4 to 10^5. Although the fluctuating velocity is expected to have some three-dimensionality, unsteady wake was dominated by coherent vortices due to the vortex shedding. Hence, it may be presumed that the decrease in the lift slope is related to the mean velocity defect and coherent velocity fluctuations in the wake.

However, a recent work [11] showed that artificially generated "homogeneous and isotropic" freestream turbulence (up to 15% in intensity) can also produce the same effect of decreasing lift slope, with slight changes in the maximum lift coefficient. The lift slope decreased with increasing turbulence intensity in the absence of any mean velocity gradients or coherent velocity fluctuations. There were no flow field measurements, however the possibility of dynamic stall caused by the turbulent cross-stream velocity fluctuations was suggested. The flow physics of decreasing lift slope in a wake or highly turbulent freestream remains unclear.

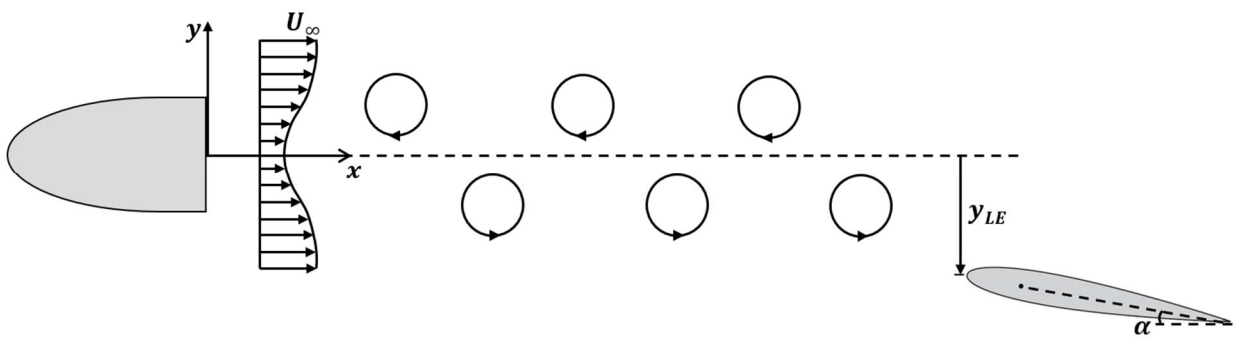

Figure 1: Schematic of the wing in the wake of a bluff body.

Previous studies of wake-airfoil interaction [1, 9, 10] were limited to the cases of zero offset distance between the wake centerline and the leading-edge of the wing. The only work that considered the effect of nonzero offset distance is by Faure et al. [12]. It was suggested that the lift in the post-stall region may increase when the clockwise vortices induce a downwash velocity at the leading-edge of the downstream airfoil. In this paper we show that the time-averaged lift is strongly affected by the offset distance of the wing in the wake, and there is significant lift increase and delay of stall at an optimal offset distance.

II. Experimental Methods

Experiments were performed in a low-speed closed-circuit open-jet wind tunnel with a circular working section of diameter of 0.76 m and length of 1.1 m, located at the University of Bath. The wind tunnel has a maximum operating speed of 30 m/s and a freestream turbulence intensity of 0.1% at maximum operational speed. The schematic of the wing in the wake of a bluff body is shown in Figure 1. The wake generator has an elliptical leading-edge with a major-to-minor axis ratio of 4:1 and a sharp rectangular back. The wake generator, supported by two end-plates, has a length of 90 mm, thickness of H = 50 mm and span of 600 mm. The downstream wing is of NACA 0012 profile with a chord length of c = 100 mm and span of b = 400 mm (equivalent of aspect ratio of 8 for this half-model). The wing and load cell assembly was mounted on a two-axis traverse that features two translation rails for the x- and y- axis adjustments (see Figure 2). For this paper, the wing leading-edge was fixed at a streamwise

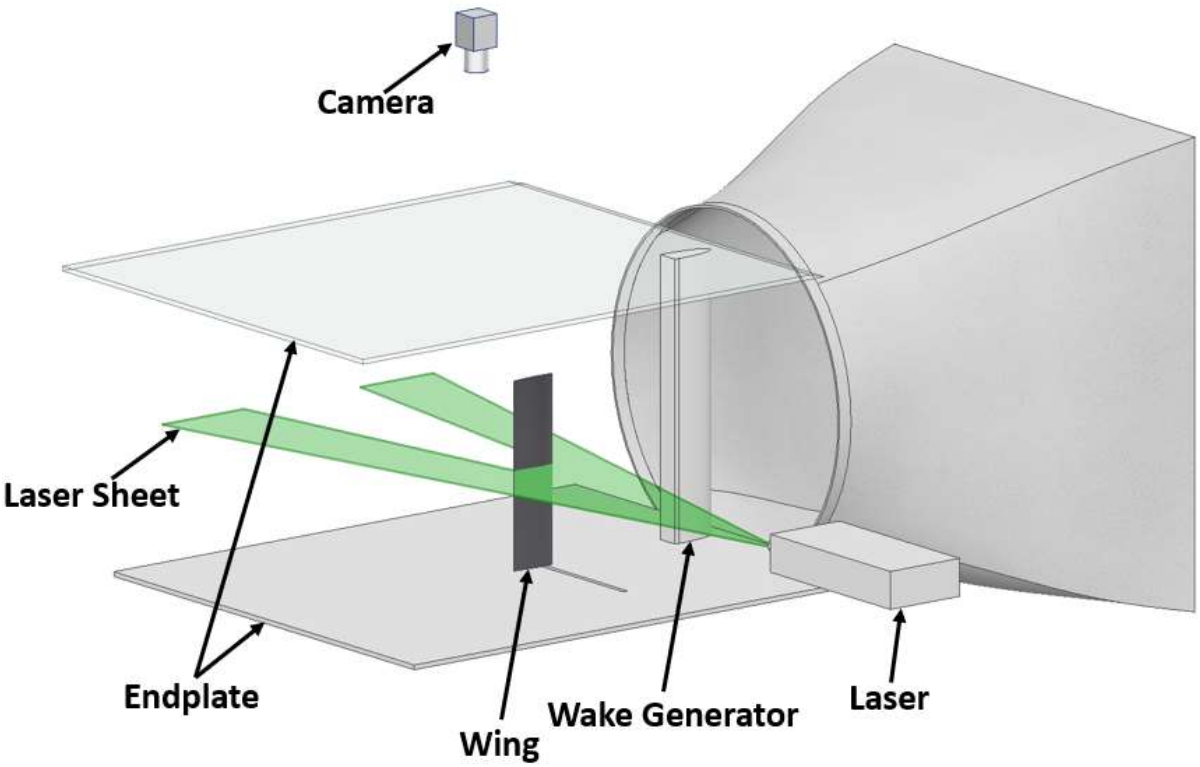

Figure 2: Schematic of the experimental setup and the PIV measurements.

distance of x/c = 3.0. All measurements were conducted at a constant freestream velocity of U_∞ = 15 m/s, corresponding to a Reynolds number based on the chord length of Re = 100,000. The wake Reynolds number based on the thickness of the bluff body was 50,000.

The wing was mounted vertically to the two-axis traverse via an aluminium binocular strain gauge force balance. The signal from the force balance is amplified through an AD624 instrumentation amplifier and logged to a personal computer via NI6009 DAQ at a sampling rate of 5 kHz. The duration of each record was 20 s, which is sufficiently long for the mean and the rms of the signal to reach a steady state value.

The Particle Image Velocimetry measurements were carried out with a TSI 2D-PIV system in the mid-span plane of the wing as sketched in Figure 2. The flow is seeded with olive oil droplets, 1 μm in diameter produced by a TSI 9307-6 automizer. The seeding particles were illumined by a NewWave Solo 120-15 Hz double pulse laser system, which has an output of 120 mJ per pulse. The laser pulse was synchronised with 8 MP Powerview plus CCD camera via the Laserpluse 610036 synchroniser. The commercial software package Insight 4G and a Hart cross-correlation algorithm were used to analyse the images. For the image processing, an interrogation window size of 32x32 pixels was used. The effective grid size was around 2 mm (2% of chord length). For each run, 2,000 instantaneous flow fields were captured at a rate of 1 Hz.

III. Results

The flow downstream of the wake generator is first examined by velocity measurements in the absence of the downstream wing. The time-averaged normalized streamwise velocity defect and root-mean-square of streamwise and cross-stream velocity fluctuations at x/c = 3.0 are presented in Figure 3(a). A normalized streamwise velocity defect of 21% is seen at the wake centerline. The rms of both streamwise and cross-stream velocity is comparable in magnitude. At x/c = 3, the wake lengthscale (location of the half defect velocity) is found to be $L_0 = 0.32c$ and the momentum thickness $\theta = 0.14c$. The proper orthogonal decomposition (POD) analysis was performed using the commercial software TSI GRAD-POD TOOLBOX. Figure 3(b) shows the first two most energetic vorticity modes (24% and 21% of the total energy), hence the coherent vortices have roughly half of the total kinetic energy in the wake. The wavelength of the coherent vortical structures is estimated as $\lambda_\infty = 1.58c$. The frequency of the Karman street, as measured by a hot-wire probe (not shown here), revealed that $fH/U_\infty = 0.26$ and $fc/U_\infty = 0.52$.

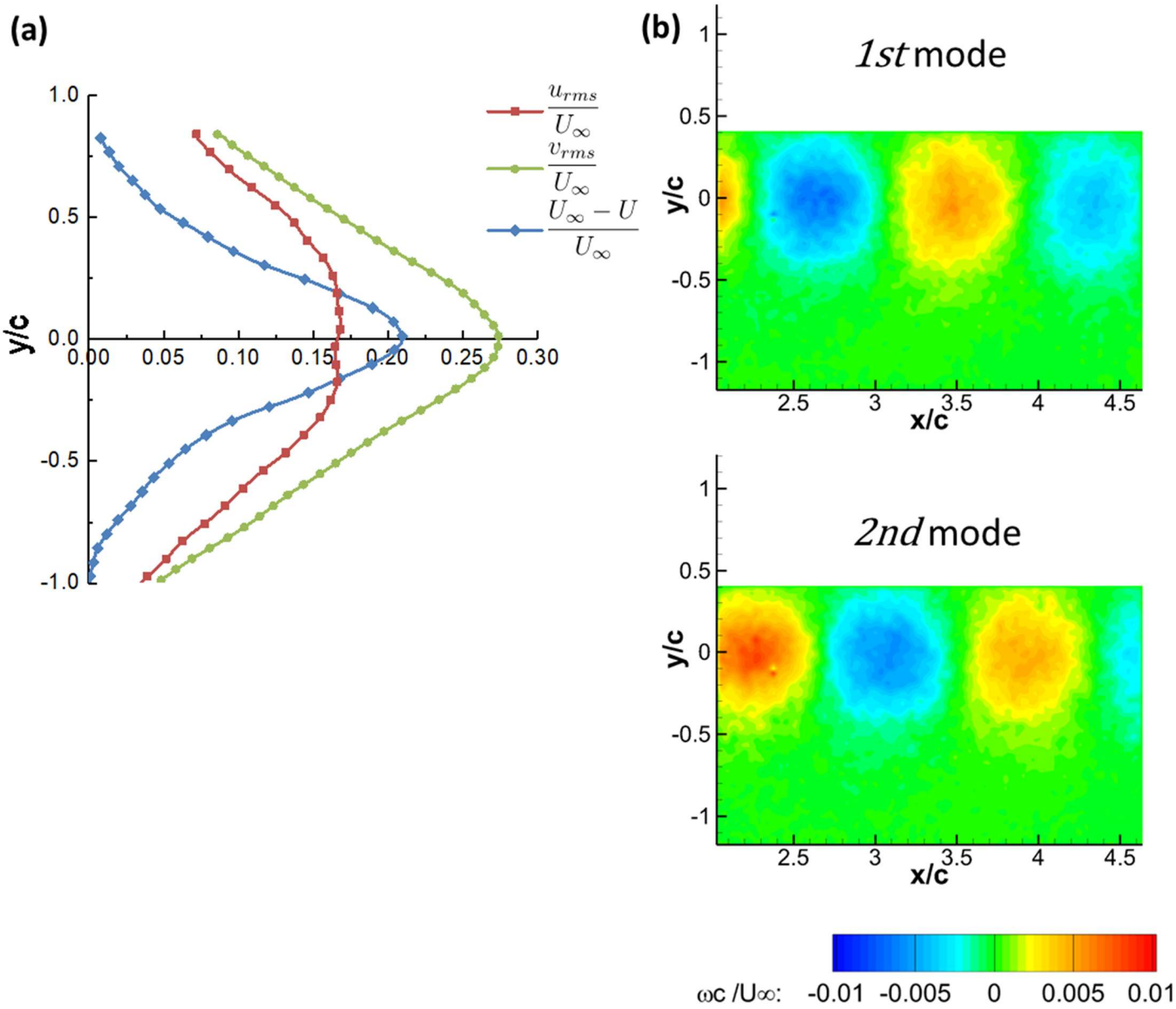

Figure 3: (a) Mean streamwise velocity defect, and rms velocity of streamwise and cross-stream velocity fluctuations at *x/c* = 3.0; (b) first two vorticity modes of the POD analysis.

Figure 4 presents the variation of the time-averaged lift coefficient C_L with the angle of attack for the wing location $x_{LE}/c = 3$ and of $y_{LE}/c = 0$ and -0.7 as well as in the freestream. The slopes of all cases around $\alpha = 0°$ agree well with the Prandtl's lifting line theory, assuming an elliptical circulation variation and using a slope of 2π for the airfoil lift coefficient. The wing when located in the wake exhibits higher maximum lift coefficient and a delay of stall. The lift enhancement can be more substantial when an offset from the wake centerline is introduced. The maximum lift coefficient, for an offset of $y_{LE}/c = -0.7$, is $C_{L,max} \approx 0.97$ at $\alpha = 20$ deg, which is 34% higher than that of the freestream case. Also, for this offset, the lift curve remains unaffected until the stall of the baseline case.

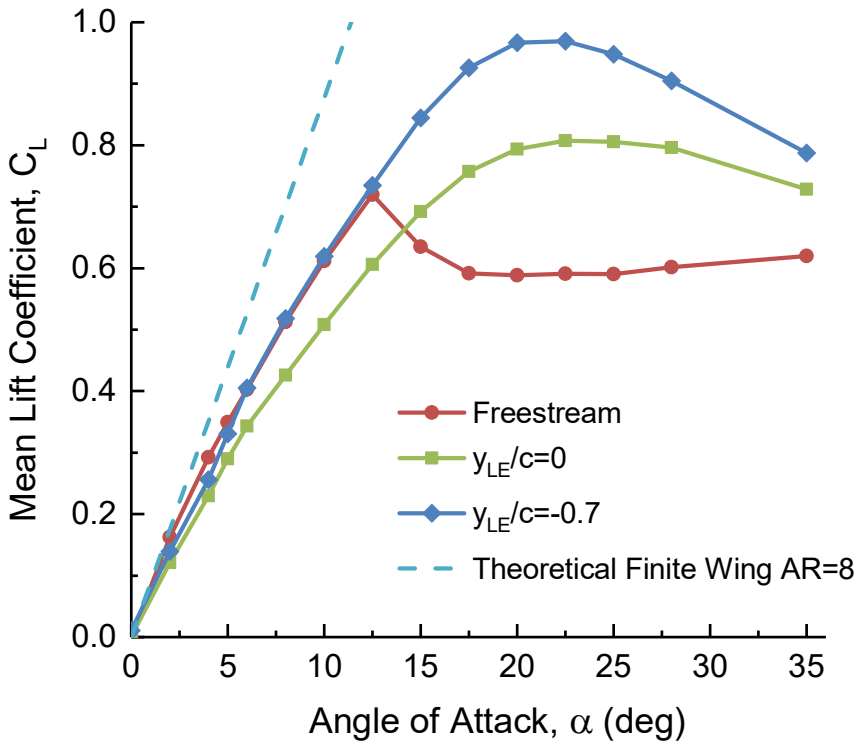

Figure 4: Mean lift coefficient as a function of angle of attack, x_{LE}/c = 3.0.

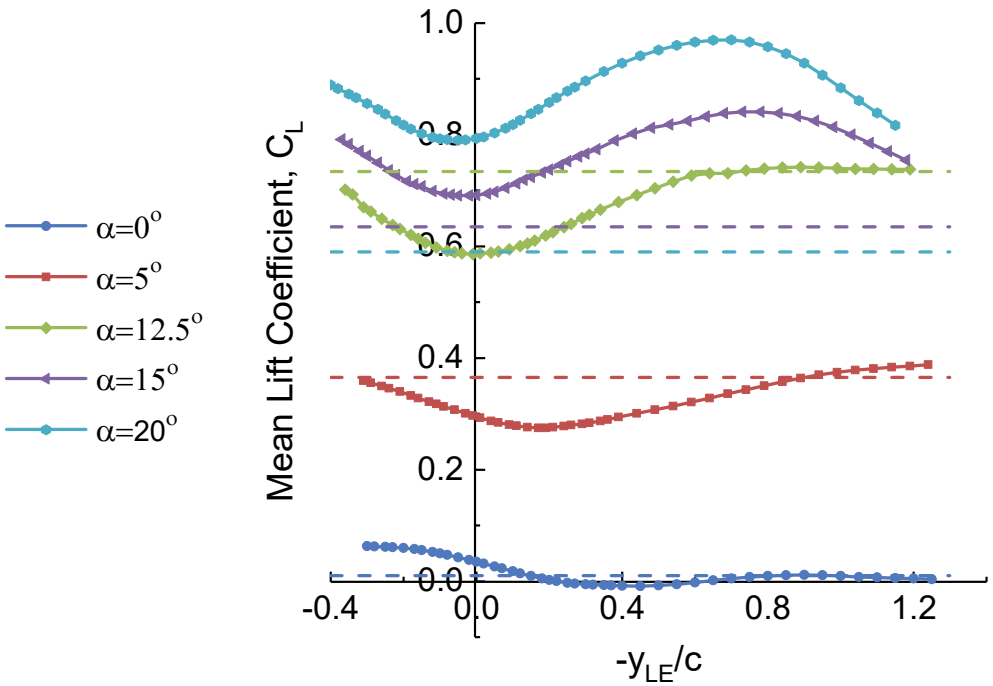

Figure 5: Mean lift coefficient as a function of offset distance from the wake centreline, x_{LE}/c = 3.0.

Figure 5 shows the variation of the time-averaged lift coefficient C_L with offset distance at various angles of attack. The dashed lines represent the lift coefficient in the freestream for the corresponding angles of attack. It is seen that below the stall angle of attack of the baseline case ($\alpha \leq 12.5$ deg), the lift coefficient experiences a drop near the wake centerline before recovering to the freestream value with increasing offset distance. In contrast, in the post-stall regime, significant lift enhancement is seen for all offset locations. In addition, there exists an optimal location at which the mean lift is maximum for both α=15 and 20 deg. The optimal location is roughly $y_{LE}/c = -0.7$ for α=20 deg, resulting in a maximum lift coefficient which is 64% larger than that of the freestream case at the same angle of attack and 34% larger than the maximum lift coefficient of the baseline wing. This offset distance also results in an increased lift near the maximum value for α=15 deg.

To understand the underlying differences in the mean flow for these cases, the time-averaged velocity measurements are presented in Figure 6 for α =15 and 20 deg at zero and the optimal offset as well as the baseline case in freestream. At $\alpha = 15$ deg in the freestream, large separated region is observed on the suction side of the wing, whereas attached (or weakly separated) flow in the time-averaged sense is observed when the wing is in the wake. At $\alpha = 20$ deg, massively separated flow is seen for the freestream case. In contrast, when the wing is in the wake, a small separation bubble near the trailing-edge for $y_{LE}/c = 0$ and a large separation bubble on the whole wing for $y_{LE}/c = -0.7$ are observed. The large separation bubble covering the entire suction surface is responsible for the significant lift enhancement. It is well known that highly curved streamlines over an airfoil, whether caused by a vortex or a separation bubble, increase the lift force. It may be assumed that the lift enhancement is directly related to the size of the separation bubble, hence the proportion of the surface of the airfoil affected by the flow curvature.

Figure 7 presents various instantaneous flow images for $\alpha = 20$ deg and $y_{LE}/c = -0.7$. For "conditional sampling", we studied the variation of the velocity magnitude just above the leading-edge region (x/c=3.1 and 0.1c above the wing surface). Figure 7(a) presents the histogram of the probability of the normalized velocity magnitude $\sqrt{u^2 + v^2}/U_\infty$ at this location. The highest probability (25%) is seen around $\sqrt{u^2 + v^2}/U_\infty = 1.3$. In Figure 7(b), we present three representative velocity and vorticity magnitude fields that satisfy the condition $1.25 < \sqrt{u^2 + v^2}/U_\infty < 1.35$ at the sampling location. Vorticity shedding and roll-up, resulting in reattachment at various chordwise locations or highly curved streamlines over the wing, and

subsequent separation in some cases, are observed. Leading-edge vortex formation and shedding becomes more pronounced for a higher velocity magnitude band $1.45 < \sqrt{u^2 + v^2}/U_\infty < 1.55$ in part (c). It is observed that within this velocity magnitude band, the reattachment locations are mainly around the mid-chord and the reattached flow subsequently separates. The instantaneous flow images in Figure 7 are similar to those of "dynamic stall" of oscillating wings [13].

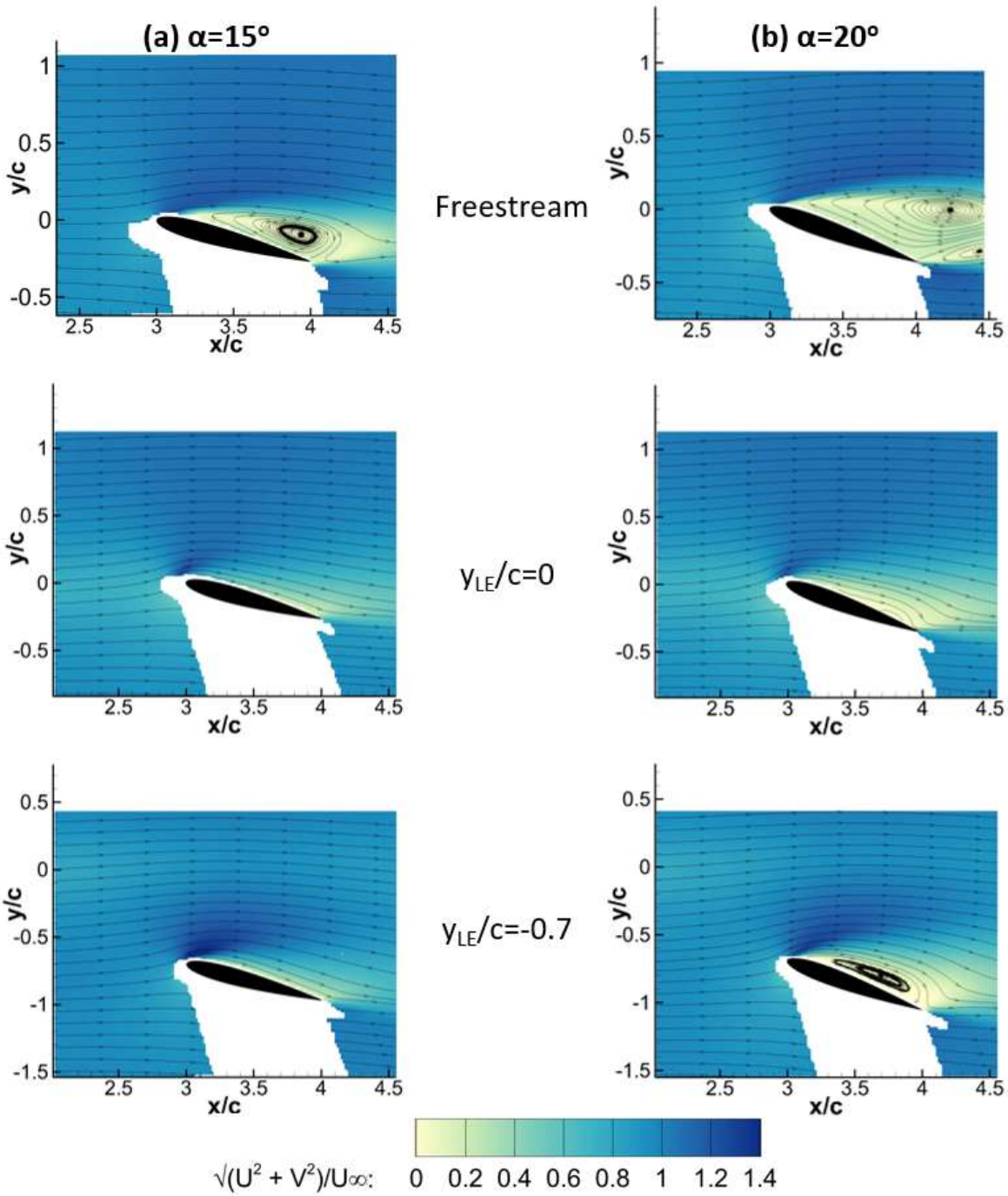

Figure 6: Mean velocity magnitude and streamlines for two locations in the wake at x_{LE}/c = 3.0 and in the freestream for α= 15° and 20°.

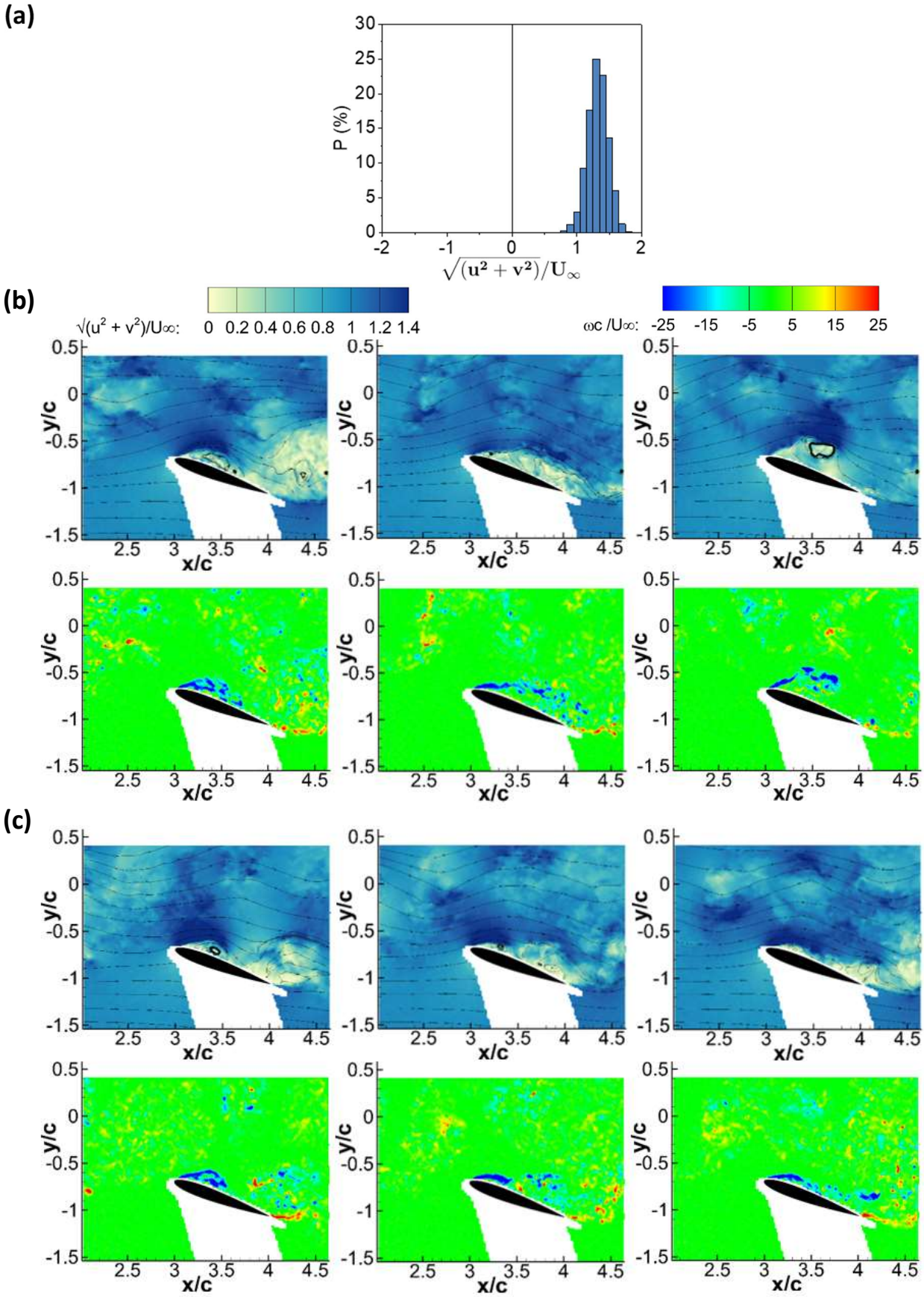

Figure 7: For α= 20° and y_{LE}/c = –0.7, (a) probability of normalized velocity magnitude above the leading-edge; (b) three images of instantaneous velocity magnitude and vorticity for normalized velocity magnitude between 1.25 and 1.35; (c) between 1.45 and 1.55.

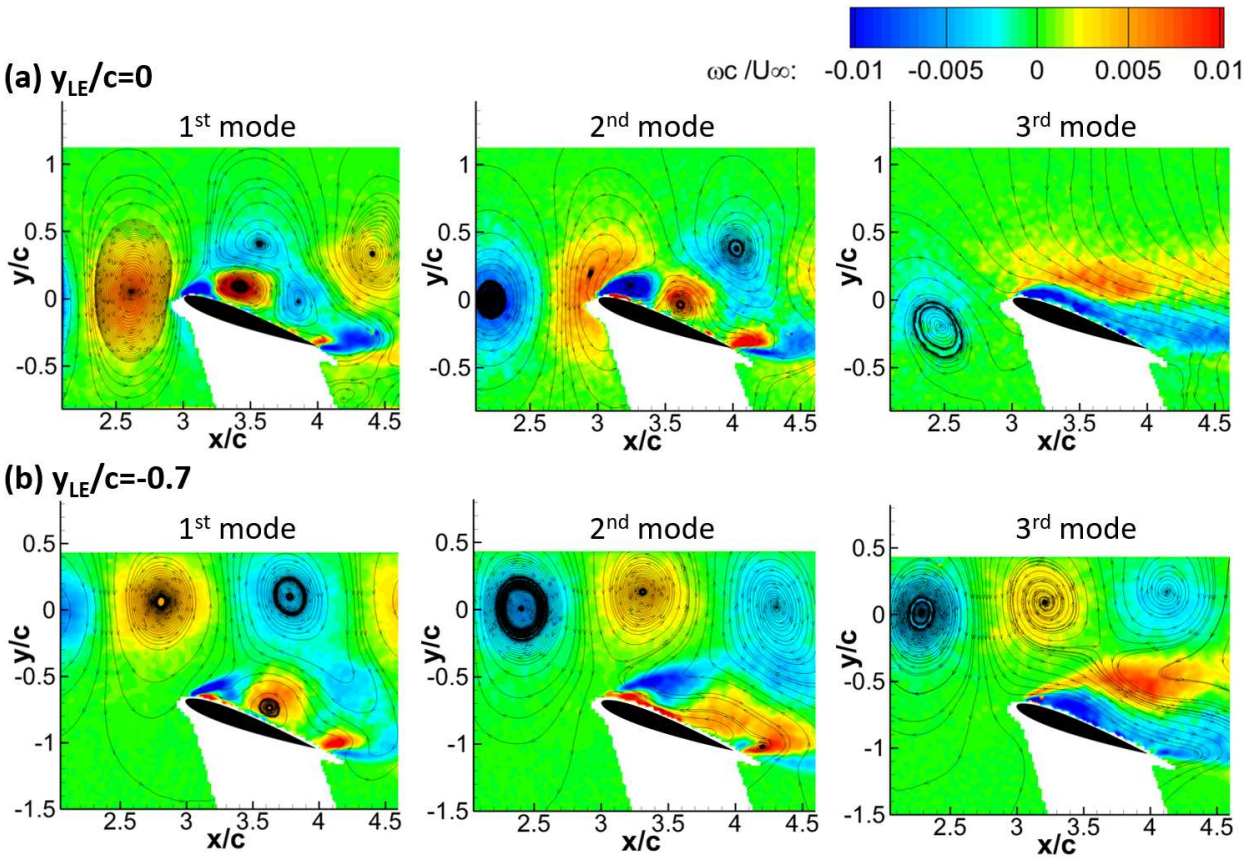

Figure 8: The first three vorticity POD modes for α= 20° and (a) y_{LE}/c = 0, (b) y_{LE}/c = –0.7.

The first three vorticity POD modes for α= 20° are compared in Figure 8 for (a) y_{LE}/c = 0, (b) y_{LE}/c = –0.7. The percentages of the total energy of the first three modes are 14.8%, 14.1% and 11.1% respectively for y_{LE}/c = 0, and 9.6%, 8.2% and 6.5% for y_{LE}/c = –0.7. For the zero offset case, the first two modes characterize the head-on collision of the vortical structures, which suggests the formation of the leading-edge vortices and separation bubbles of different sizes. The third mode represents the flapping of the shear layer. For the optimal offset case, there are similar POD modes, although the flow separation is induced by the oscillations in the potential flow region, not by the direct impingement of the vortices.

Figure 9 compares the probability of the local wake angle $\alpha_{wake} = tan^{-1}(v/u)$, which provides an indication of the local angle of attack of upstream flow, as well as its time rate, called "reduced pitch rate", at y/c = 0 and -0.7 in the absence of the wing. At the wake centreline (y/c=0), the probability of the wake angle is distributed symmetrically about α_{wake} = 0 deg. Slightly higher probability is seen around α_{wake} = ±20 deg than at α_{wake} = 0, which is due to the sinusoidal variation of wake angle due to the passage of the vortices. At the optimal cross-stream location (y/c=-0.7), there is an asymmetry of the histogram with higher probability at a positive wake

angle of around 3 deg, but the mean wake angle is very small (0.6 deg). For the reduced pitch rate $K = c(d\alpha_{wake}/dt)/2U_\infty$, the time rate $d\alpha_{wake}/dt$ was calculated by using the Taylor's hypothesis and a high-order central differencing to find dv/dx. Figure 9 shows that the reduced pitch rate exhibits a narrower probability distribution at the optimal location than the wake centreline. While small scale structures are associated with larger values of K, it can be estimated that large-scale Karman street vortices produce $K \approx 0.18$ at the centerline, which is large enough to cause dynamic stall vortices [13]. On the other hand, higher probability of velocity oscillations at smaller amplitudes, with sufficiently high time rates, at the optimal location is reminiscent of periodic excitation for active flow control. It is known from the active flow control experiments that the optimal Strouhal number of the excitations is in the range of $fc/U_\infty = 0.5$ to 1.0 [14], which is consistent with the value of 0.52 in our experiments.

The time-averaged velocity measurements presented in Figure 6 reveal that the optimal location causes highly curved streamlines forming a closed separation bubble in the time-averaged sense. The reattachment of the flow in the region of the trailing edge is similar to other high-lift producing flows in the cases of unsteady freestream [15] and active flow control with suction [16]. This type of flow is not observed when the wing is placed at the centreline. Hence, the mean streamline pattern is well correlated with the enhanced time-averaged lift. However, it is not clear how the smaller amplitude excitation at the optimal location (in comparison to the larger amplitude excitation at the wake centreline) leads to the optimal time-averaged flow. This remains to be studied.

We believe that the mechanism of lift enhancement at a post-stall angle of attack is similar to that observed in other unsteady flows. Early studies of streamwise velocity fluctuations in a freestream [15] showed that the mean lift becomes maximum at an optimal frequency. The simplest simulation of uniform transverse fluctuations is a plunging airfoil [17], which is known to produce enhanced lift at optimal frequencies. Unsteady disturbances produced by a gust generator are likely to increase the mean lift, provided that frequency is appropriately tuned. However, gust generators are likely to require external power, whereas wakes of stationary bodies provide unsteady disturbances that do not require external power.

Finally, the effect of three-dimensionality remains to be studied. Our experiments were performed at a Reynolds number based on the bluff body thickness $Re = 50{,}000$ and for $x/H = 6$. At a comparable Reynolds number based on the diameter $Re = 13{,}000$ and in the intermediate wake region $x/d = 20$, Hayakawa and Hussain [18] found significant three-dimensionality and

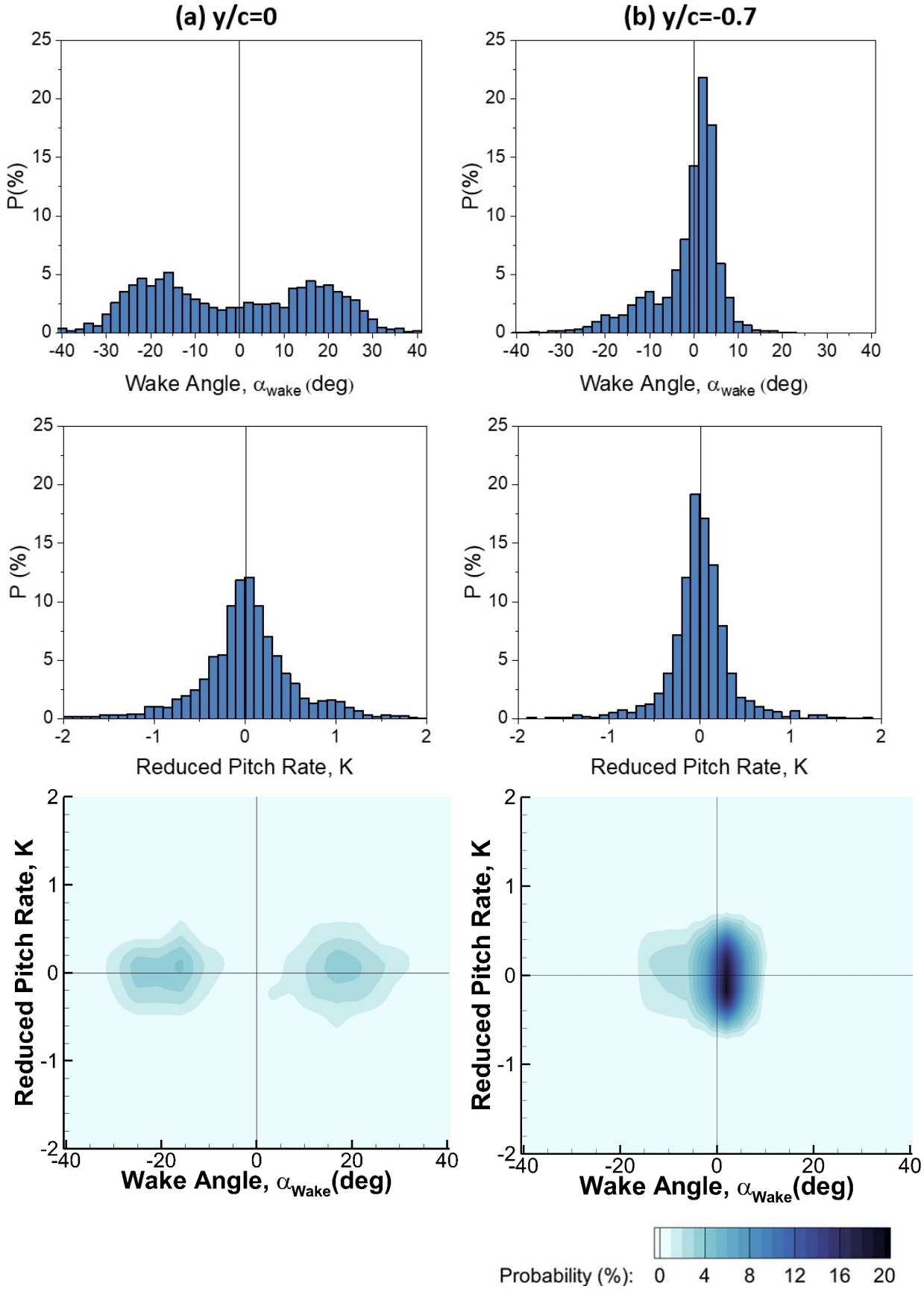

Figure 9: Probability of wake angle α_{wake}, probability of reduced pitch rate *K*, and joint probability of wake angle and reduced pitch rate at (a) *y/c* = 0, (b) *y/c* = –0.7.

estimated the spanwise scale of vortical structures around 1.8*d*. They concluded that the typical spanwise extent of large spanwise vortices is comparable with the local half-width of the wake. We are investigating this aspect further and would like to report on it in the near future.

IV. Conclusions

The unsteady aerodynamics of a wing placed in a wake of a bluff body was investigated. Lift force measurements revealed that the wing experienced mean lift enhancement as well as a delay of stall compared to the freestream. The lift enhancement at the post-stall angles of attack became maximum when the wing was placed at an optimal offset distance from the wake centreline. A 34% increase in the maximum lift coefficient and delay of stall angle of 9° was observed. The increased lift is due to the flow separation and formation of a large separation bubble in the time-averaged flow. The instantaneous flow revealed that the quasi-periodic wake flow excites the separated flow and causes the formation of leading-edge vortex and reattachment, similar to the dynamic stall of oscillating wings. At the optimal location, small amplitude oscillations, as opposed to the large amplitude oscillations at the wake centerline, provide an effective way for flow control. Even though the excitation frequency in this case is in the range of optimal flow control frequencies, the excitation is believed to have low spanwise correlation at this wake Reynolds number, which makes this finding intriguing.

Acknowledgements

The authors acknowledge the Engineering and Physical Sciences Research Council (EPSRC) strategic equipment grant funding (EP/K040391/1).

References

[1] Scharpf, D. F., and Mueller, T. J., "Experimental Study of a Low Reynolds Number Tandem Airfoil Configuration", *Journal of Aircraft*, Vol. 29, No. 2, 1992, pp. 231–236. https://doi.org/10.2514/3.46149

[2] Lissaman, P. B. S., and Shollenberger, C. A., "Formation Flight of Birds", *Science*, Vol. 168, No. 3934, 1970, pp. 1003-1005. https://doi.org/10.1126/science.168.3934.1003

[3] Lehmann, F.O., "Wing–Wake Interaction Reduces Power Consumption in Insect Tandem Wings", *Experiments in Fluids*, Vol. 46, 2009, pp. 765–775. https://doi.org/10.1007/s00348-008-0595-0

[4] Boschitsch, B. M., Dewey, P. A., and Smits, A. J., "Propulsive Performance of Unsteady Tandem Hydrofoils in an In-Line Configuration", *Physics of Fluids*, Vol. 26, 2014, Paper 051901. https://doi.org/10.1063/1.4872308

[5] Allen, J., Techet, A., Kelso, R., and Smits, A., "Energy Harvesting Eel", *Journal of Fluids and Structures,* (2001) 15, pp. 629-640.
https://doi.org/10.1006/jfls.2000.0355

[6] Hodson, H. P., and Howell, R. J., "Bladerow Interactions, Transition, and High-Lift Aerofoils in Low-Pressure Turbines", *Annual Review of Fluid Mechanics*, Vol. 37, 2005, pp. 71–98.
https://doi.org/10.1146/annurev.fluid.37.061903.175511

[7] Rockwell, D., "Vortex-Body Interactions", *Annual Review of Fluid Mechanics*, Vol. 30, No. 1, 1998, pp. 199–229
https://doi.org/10.1146/annurev.fluid.30.1.199

[8] Gursul, I., and Rockwell, D., "Vortex Street Impinging upon an Elliptical Leading Edge," *Journal of Fluid Mechanics*, Vol. 211,1990, pp. 211–242.
https://doi.org/10.1017/s0022112090001550

[9] Durgesh, V., Padilla, R., Garcia, E. N., and Johari, H., "Impact of Coherent Structures on Aerodynamics Performance at Low Reynolds Numbers", AIAA Paper 2019-0847, AIAA ScitTech 2019 Forum, 2019.
https://doi.org/10.2514/6.2019-0847

[10] Lefebvre, J. N., and Jones, A. R., "Experimental Investigation of Airfoil Performance in the Wake of a Circular Cylinder", *AIAA Journal*, 2019, pp. 2808–2818.
https://doi.org/10.2514/1.j057468

[11] Kay, N. J., Richards, P. J., and Sharma, R. N., "Influence of Turbulence on Cambered and Symmetrical Airfoils at Low ReynoldsNumbers", *AIAA Journal*, 2019, pp. 1–13.
https://doi.org/10.2514/1.J058822

[12] Faure, T. M., Hétru, L., and Montagnier, O., "Vortex Dynamics Resulting from the Interaction Between Two NACA 23012 Airfoils", Proceedings of the 50th 3AF International Conference on Applied Aerodynamics, Toulouse, France, 2015.
www.3af-aerodynamics2015.com

[13] Ekaterinaris, J., and Platzer, M., "Computational Prediction of Airfoil Dynamic Stall," *Progress in Aerospace Sciences*, Vol. 33, Nos. 11-12, 1998, pp. 759–846.
https://doi.org/10.1016/S0376-0421(97)00012-2

[14] Greenblatt, D., and Wygnanski, I. J., "The Control of Flow Separation by Periodic Excitation", *Progress in Aerospace Sciences*, Vol. 36, No. 7, 2000, pp. 487–545.
https://doi.org/10.1016/S0376-0421(00)00008-7

[15] Gursul, I. and Ho, C.-M., "High Aerodynamic Loads on an Airfoil Submerged in an Unsteady Stream", *AIAA Journal*, Vol. 30, No. 4, April 1992, pp. 1117-1119.
https://doi.org/10.2514/3.11034

[16] Wang, Z. and Gursul, I., "Lift Enhancement of a Flat-Plate Airfoil by Steady Suction", *AIAA Journal*, 2017.
https://doi.org/10.2514/1.J055382

[17] Cleaver, D.J., Wang, Z., Gursul, I. and Visbal, M.R., "Lift Enhancement by Means of Small-Amplitude Airfoil Oscillations at Low Reynolds Numbers", *AIAA Journal*, Vol. 49, No. 9, September 2011, pp. 2018-2033. https://doi.org/10.2514/1.J051014

[18] Hayakawa, M. and Hussain, "Three-dimensionality of organized structures in a plane turbulent wake", *Journal of Fluid Mechanics*, vol. 206, 1989, pp. 375-404 https://doi.org/10.1017/S0022112089002338